Mechanism of reversible transformation-induced plasticity of Fe–Mn–Si shape memory alloys

Takahiro Sawaguchi,[a,*] Leandru-Gheorghe Bujoreanu,[b] Takehiko Kikuchi,[a] Kazuyuki Ogawa,[a] Motomichi Koyama[a,c] and Masato Murakami[c]

[a]Innovative Materials Engineering Laboratory, National Institute for Materials Science, 1-2-1 Sengen, Tsukuba, Ibaraki 3050047, Japan
[b]Faculty of Material Science and Engineering, "Gh. Asachi" Technical University from Iaşi, Bd. D. Mangeron 61A, 700050 Iaşi, Romania
[c]Shibaura Institute of Technology, Tokyo 135-8548, Japan

The mechanism of reversible transformation-induced plasticity of an Fe–30Mn–6Si (mass %) shape memory alloy, under tensile stress and subsequent compression, has been observed by optical and atomic force microscopy. The tensile stress-induced ε (hexagonal close-packed) martensite reverts into γ (face-centered cubic) austenite after compression to zero strain. Further compression to negative strains induces a different ε martensite variant from that of the tensile-stress-induced ε martensite.
© 2008 Acta Materialia Inc. Published by Elsevier Ltd. All rights reserved.

After the discovery of the one-way shape memory effect (SME) in Fe–30Mn–1Si (mass %) single crystals by Sato et al. [1], polycrystalline alloys with almost perfect SME were developed by Murakami et al. based on Fe–30Mn–6Si (hereafter all compositions are in mass %), undergoing the γ (face-centered cubic: fcc) $\leftrightarrow$ ε (hexagonal close-packed: hcp) martensitic transformation [2].

Aiming to further develop these shape memory alloys (SMAs), considerable efforts were made to induce corrosion resistance, by alloying with Cr and Ni [3], and to improve the SME, by microalloying [4–6], training [7] or NbC precipitation [8,9]. In this way, SMAs with good workability and reasonable cost have been developed. The alloys are suitable for constrained recovery applications [10], such as pipe joints [11] and rail couplings [12].

Recently, some of the present authors reported that an Fe–28Mn–6Si–5Cr–0.5NbC SMA showed significant damping capacity when subjected to cyclic tension–compression loading with strain amplitudes larger than 10^{-3}. The result indicates the capability of the SMA for new potential vibration-absorbing applications such as anti-seismic dampers for large structural bodies. Buildings and other structures can be protected against earthquakes by anti-seismic dampers made from low yield point (LYP) steels [13]; however, Fe–Mn–Si-based SMAs would be superior since they have lower cyclic hardening rate, probably due to the reversible $\gamma \leftrightarrow \varepsilon$ transformation during cyclic tension–compression loading [14]. Quantitative X-ray diffraction analysis and atomic force microscopy (AFM) performed in our previous report [14] proved that reverse martensitic transformation of tensile-stress-induced martensite took place when the specimen was compressed back to zero strain. However, deformation behavior and microstructure evolution after further compression to negative strains are still unclear.

The present study aims to establish a detailed deformation mechanism of Fe–Mn–Si SMAs under tension–compression loading. Taking into account that the reversible character of γ/ε interface movement, during tension and compression, was previously observed by some of the present authors in the specific case of an Fe–28Mn–6Si–5Cr–0.5NbC SMA, the presence of the above reversibility was confirmed for the "conventional" Fe–30Mn–6Si SMA. The evolution of the defor-

---

* Corresponding author. E-mail: sawaguchi.takahiro@nims.go.jp

mation microstructure of the SMA, during the deformation path from a tensile strain through zero strain to a compressive strain, was observed by combined use of optical microscopy and AFM.

After induction melting, hot forging, hot rolling and solution treatment (1270 K/3 h/water) under argon atmosphere, specimens with gauge dimensions $3 \times 4 \times 20 \times 10^{-3}$ m (for tension–compression tests), as well as internal friction (IF) specimens, with dimensions $1 \times 5 \times 50 \times 10^{-3}$ m were cut by spark-erosion. The chemical composition was determined by spectrogravimetry as: 30.08% Mn, 6.08% Si, 0.007% C, 0.002% P, 0.008% S, 37 ppm N, bal. Fe.

IF and storage modulus measurements were performed by means of a dynamic mechanical analyzer (DMA) in order to determine critical temperatures for both martensitic and antiferromagnetic transformations, between 570 and 130 K. DMA measurements revealed a forward martensitic transformation, $\gamma \rightarrow \varepsilon$, on cooling below $M_s = 342$ K, critical temperature for transformation start and a reverse martensitic transformation, $\varepsilon \rightarrow \gamma$, on heating between $A_s = 393$ K and $A_f = 459$ K, critical temperatures for reversion start and finish, respectively. In addition, an obvious paramagnetic $\rightarrow$ antiferromagnetic transition was noticed, characterized by a Néel temperature ($T_N = 256$ K) estimated by the starting point of modulus decrease on cooling [15].

Tensile testing specimens were elongated to a permanent strain of 3.3%, at room temperature (RT), on a tensile testing machine, in order to obtain tensile-stress-induced ε martensite, designated as $\varepsilon_{(T)}$. Then, lateral fixing extremities were cut and the specimens were first compressed back to a permanent strain of -0.2% and further to -2.0% strain, where compressive-stress-induced martensite, $\varepsilon_{(C)}$, would be formed. The characteristics of stress-induced martensite plates in the three above-mentioned states, (i) 3.3% extended, (ii) compressed back to -0.2% and (iii) -2.0% compressed, were analyzed, by differential-interference optical microscopy (OPM) and AFM in order to reveal the reversible character of stress-induced martensite plate movement, during plastic tension–compression. Details for DMA, OPM and AFM experiments were provided previously [14,16,17].

Differential-interference OPM revealed the reversibility of stress-induced martensitic transformation in the Fe–30Mn–6Si SMA, demonstrating that, when changing deformation character from tension to compression, ε-martensite plates also modify their thickness and orientation, as shown in Figure 1. In Figure 1a, the OPM micrograph of a central grain is shown in elongated state characterized by a permanent tensile strain of 3.3%. The grain includes two twins which were previously observed by OPM on mechanically polished and subsequently etched surface. Considering their widths, of the order of tens of micrometers, and the fact that no grain boundary distortion is noticeable at their level, it is assumed that they were not formed by deformation but by annealing [18]. It is obvious that, as a consequence of plastic deformation by extension, plate-like tensile-stress-induced martensite $\varepsilon_{(T)}$ was formed, both in parent and in annealed twin crystals. It is worth noting that, in the parent areas of the crystal, the plates belong mostly to a single crystallographic variant of martensite
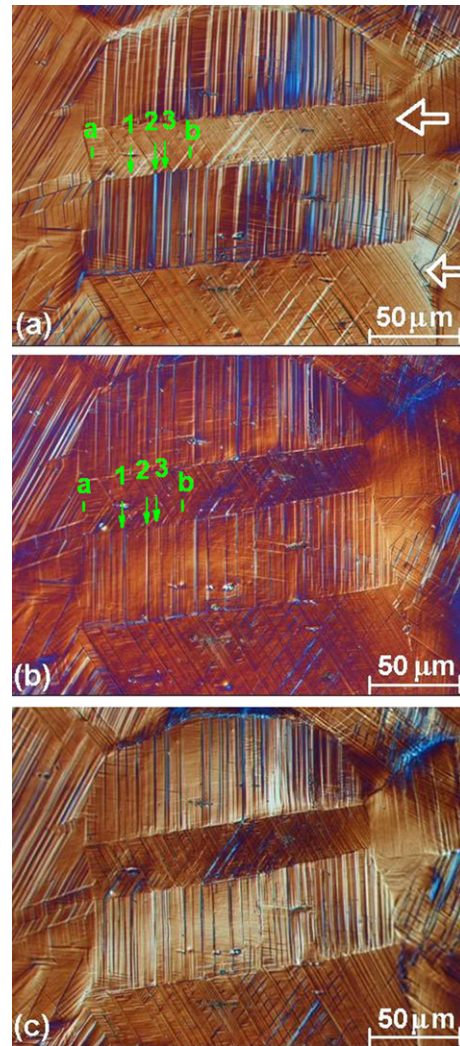
Figure 1. Differential-interference OPM micrographs illustrating the evolution of ε stress-induced martensite plates, at three consecutive plastic deformation stages during a tension–compression cycle: (a) elongated by 3.3%; (b) compressed back to -0.2%; (c) further compressed to -2.0%.

with a unique $\{111\}_\gamma$ habit plane, which from the point of view of Schmid's law is most preferably oriented with respect to deformation axis. In the twinned area of the crystal, secondary $\varepsilon_{(T)}$ variants with a different $\{111\}_\gamma$ habit plane are also visible. After compression back to -0.2% strain, Figure 1b shows that the thickness of $\varepsilon_{(T)}$ plates was remarkably reduced. Thus, it is rather obvious that three martensite plates, designated as 1, 2 and 3 and located between the markers a and b in the crystal area below the upper annealed twin, become narrower in Figure 1b than in Figure 1a. Moreover, the change in contrast indicates a change in orientation both in parent and twinned crystals. Further compression to -2.0% strain causes a new increase of plate thickness, in Figure 1c. Since the color of martensite plates is different between Figure 2a and c, because light is differently reflected by differently oriented surfaces, it may be assumed that martensite plates have changed their surface relief from tensile-induced to compression-induced, transforming from $\varepsilon_{(T)}$ to $\varepsilon_{(C)}$, respectively. In other words it is assumed that, within the above-men-
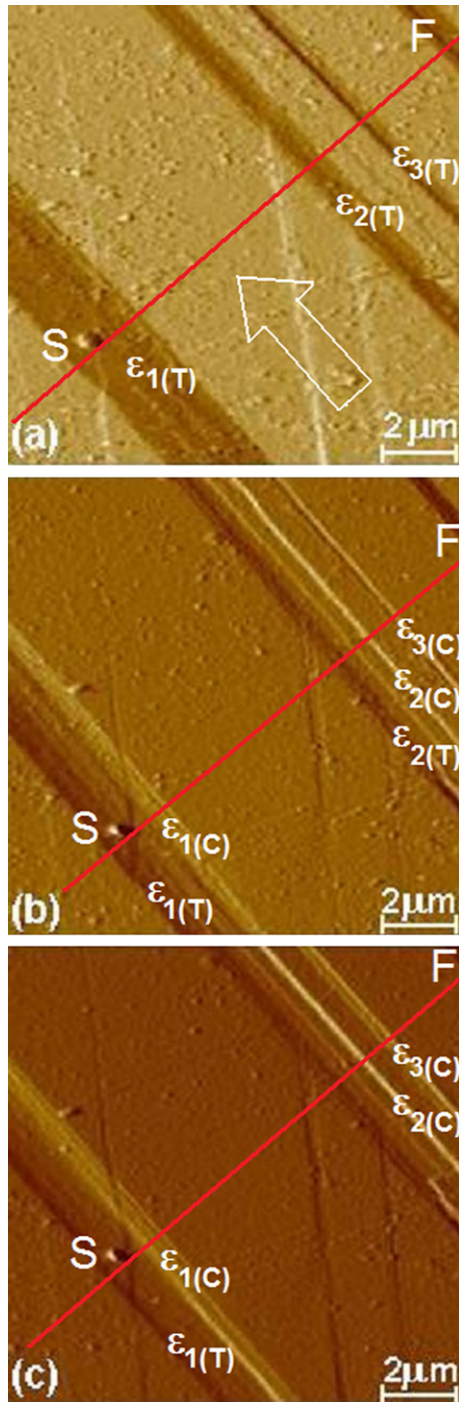
Figure 2. AFM micrographs illustrating the reversible movement of three ε stress-induced martensite plates, at the same stages represented in Figure 1, during a tension–compression cycle: (a) elongated by 3.3%; (b) compressed back to −0.2%; (c) further compressed to −2.0%.

tioned strain limits, Fe–30Mn–6Si SMA shows reversible plastic deformation associated with reversible stress-induced martensitic transformation.

The reversible character of the transformation-induced plasticity in Fe–30Mn–6Si is further demonstrated in Figure 2 by three AFM micrographs. By means of an analytical method detailed elsewhere [19], the plate-like products corresponding to tension-induced, $\varepsilon_{(T)}$, and compression-induced, $\varepsilon_{(C)}$, martensite plates as well as

to γ-austenite were identified. Figure 2a shows the surface relief image of the specimen elongated to 3.3%. Along the line S–F in Figure 2a there are three wide γ-plates, light in color, and three visible tension-induced martensite plates, $\varepsilon_{1(T)}$, $\varepsilon_{2(T)}$ and $\varepsilon_{3(T)}$, dark in color. After compression back to −0.2% strain, the general color of surface relief changed in Figure 2b, indicating a common rotation of the entire area. However, the left-hand side parts of the plates designated by the coefficients 1 and 2 maintained their general dark contrast so it may be assumed that these parts preserved their initial orientation. Therefore they are further designated as $\varepsilon_{1(T)}$ and $\varepsilon_{2(T)}$. Nevertheless, the color of the central parts of the plates became identical with austenite matrix while their right-hand side parts changed contrast and became bright colored. This suggests that the right-hand side parts of the initial $\varepsilon_{1(T)}$ and $\varepsilon_{2(T)}$ plates underwent a marked orientation change and turned to $\varepsilon_{1(C)}$ and $\varepsilon_{2(C)}$, respectively. A similar change occurred in the case of right-hand side plate, designated with subscript 3. Its left-hand side part changed color to become almost identical to the austenitic matrix, while its right-hand side part completely changed color and became bright-colored. Therefore, it is assumed that, as a result of compressing back to 0% strain, the right-hand side parts of the three tension-induced $\varepsilon_{1(T)}$, $\varepsilon_{2(T)}$ and $\varepsilon_{3(T)}$ martensite plates, changed into compression-induced $\varepsilon_{1(C)}$, $\varepsilon_{2(C)}$ and $\varepsilon_{3(C)}$ martensite plates, respectively. At the same time, the central parts of tension-induced $\varepsilon_{1(T)}$, and $\varepsilon_{2(T)}$ as well as the left-hand side part of tension-induced $\varepsilon_{3(T)}$ reverted to austenite. The only parts that preserved their initial orientation were the left-hand side parts of tension-induced $\varepsilon_{1(T)}$ and $\varepsilon_{2(T)}$ martensite. On further compression to −2% strain, Figure 2c shows that plate $\varepsilon_{3(C)}$ preserved its color and became wider. In addition, the largest part of the ε_1 and ε_2 plates became light-colored due to the orientation change from tension-induced to compression-induced, while the overall austenitic matrix became dark colored, indicating a marked orientation change between tensioned and compressed states. Only $\varepsilon_{1(T)}$ kept its initial tension-induced orientation.

These assumptions are confirmed by the corresponding surface profiles from Figure 3. In the elongated condition, Figure 3a allows the widths of the tension-induced martensite plates $\varepsilon_{1(T)}$, $\varepsilon_{2(T)}$ and $\varepsilon_{3(T)}$ to be determined as 1720, 620 and 380 nm, respectively. By comparing Figure 3a and b it is obvious that a large portion of left-hand side part of plate $\varepsilon_{3(T)}$ changed its orientation and became parallel with the general profile of the surface, which suggests its reversion from tensile-stress-induced martensite to austenite. The adjacent region located in the right-hand side of the previous $\varepsilon_{3(T)}$ plate, in Figure 3b, changed its surface tilt angle to the opposite sense to that of $\varepsilon_{3(T)}$, turning into compression-induced martensite $\varepsilon_{3(C)}$ with a width of 130 nm. The left-hand side part of $\varepsilon_{2(T)}$ kept its orientation but its width decreased from 620 to 360 nm. On the other hand, the central part of the initial $\varepsilon_{2(T)}$ became parallel to the matrix while its right-hand side part changed its tilt angle to the opposite sense to the initial orientation and became compression-induced $\varepsilon_{2(C)}$, with a width of 90 nm. Finally, the largest part of $\varepsilon_{1(T)}$, located on the left-hand side, also kept its orientation but its width
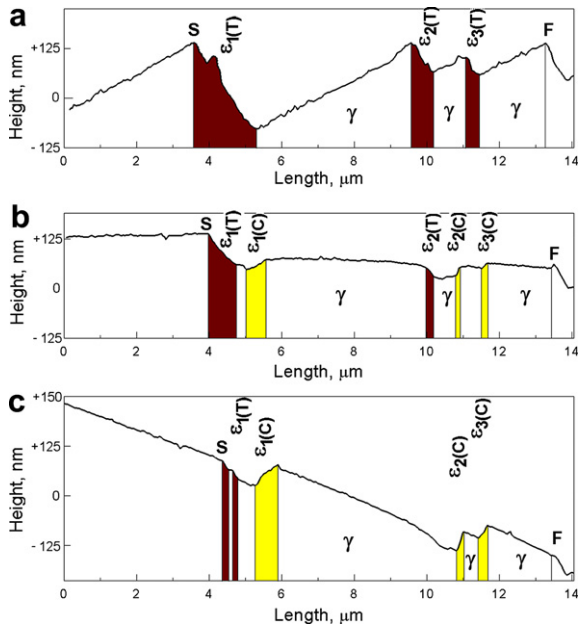
Figure 3. Surface relief corresponding to the three AFM micrographs from Figure 2: (a) elongated with 3.3%; (b) compressed back to −0.2%; (c) further compressed to −2.0%.

decreased from 1720 to 1060 nm. The central part of $\varepsilon_{1(T)}$ became parallel to general surface profile while its right-hand side part turned to compression-induced $\varepsilon_{1(C)}$ martensite with a width of 530 nm. Figure 3c shows that further compression to −2% caused plate $\varepsilon_{3(C)}$ to maintain the same tilt profile while its width increased to 220 nm. In addition, the widths of $\varepsilon_{1(C)}$ and $\varepsilon_{2(C)}$ plates increased to 620 and 200 nm, respectively. The tension-induced martensite plate $\varepsilon_{1(T)}$ became fragmented while $\varepsilon_{2(T)}$ can not be distinguished from austenitic matrix.

In case of thermoelastic SMAs, like NiTi alloys, the tension-induced martensite changes its crystallographic variant by compression. In other words, compression following extension causes direct martensite-to-martensite transformation [20,21]. On the other hand, in the present case of Fe–Mn–Si SMAs, variant transformation is accomplished in two steps consisting of the reverse martensitic transformation of the tension-induced martensite and new formation of compression-induced martensite. It is considered that the driving force of the reverse transformation, which in thermally induced transformation is associated with overheating above the thermodynamic equilibrium temperature, is given in the case of deformation-induced reverse martensitic transformation by the compression, which is in the preferable orientation for the reverse movement of Shockley partial dislocations residing at the tips of the tension-induced martensite.

In summary, the mechanism of reversible transformation-induced plasticity, during a tension–compression cycle, has been introduced, on the basis that ε martensite plates were tensile-induced with one crystallographic orientation, and then almost reverted to austenite after compression back to zero strain. Newly compression-induced martensite plates of a different crystallographic variant were formed after further compression to "negative" strains. In agreement with previously reported re-

sults, it is assumed that compression-induced martensite $\varepsilon_{(C)}$ would also reversibly transform to austenite after subsequent tension, in the same way that tension-induced martensite $\varepsilon_{(T)}$ reverts to austenite after compression [16]. These results support the conclusion that the mechanism of reversible plasticity is based on reversible tensile/compressive stress-induced martensitic transformation in the sequence $\varepsilon_{(T)} \leftrightarrow \gamma \leftrightarrow \varepsilon_{(C)}$.

[1] A. Sato, E. Chishima, K. Soma, T. Mori, Acta Metall. 30 (1982) 1177.
[2] M. Murakami, H. Otsuka, H.G. Suzuki, S. Matsuda, in: Proc. Int. Conf. Martensitic Transformation, Japan Institute of Metals, 1986, pp. 985–990.
[3] L.J. Rong, Y.Y. Li, C.X. Shi, Scripta Metall. Mater. 34 (6) (1996) 993.
[4] K. Tsuzaki, Y. Natsume, Y. Kurokawa, T. Maki, Scripta Mater. 27 (1992) 471.
[5] Bohong Jiang, Xuan Qi, Weiming Zhou, Zheng Lei Xi, T.Y. Hsu (Zuyao Xu), Scripta Mater. 34 (9) (1996) 1437.
[6] Chenxu Zhao, Gongyin Liang, Chenglao Li, Zhihao Jin, Scripta Mater. 38 (7) (1998) 1163.
[7] D.Z. Liu, S. Kajiwara, T. Kikuchi, N. Shinya, Phil. Mag. 83 (2003) 2875.
[8] S. Kajiwara, D.Z. Liu, T. Kikuchi, N. Shinya, J. Phys. IV France 11 (2001) Pr8–Pr199.
[9] Z. Dong, T. Sawaguchi, T. Kikuchi, F. Yin, K. Ogawa, P. Sahu, S. Kajiwara, Mater. Sci. Eng. 442 (2006) 404.
[10] J.L. Proft, T.W. Duerig, in: T.W. Duerig, K.N. Melton, D. Stöckel, C.M. Wayman (Eds.), Engineering Aspects of Shape Memory Alloys, Butterworth Heinemann, London, 1990, pp. 115–129.
[11] S. Kajiwara, A. Baruj, T. Kikuchi, N. Shinya, Proc. SPIE 5053 (2003) 250.
[12] A. Sato, H. Kubo, T. Maruyama, Mater. Trans. 47 (2006) 571.
[13] T. Sawaguchi, T. Kikuchi, K. Ogawa, F. Yiu, S. Kajiwara, A. Kushibe, T. Ogawa, Key Eng. Mater. 319 (2006) 53.
[14] T. Sawaguchi, K. Ogawa, T. Kikuchi, Proc. SMST 2007, Tsukuba (to be published).
[15] Y. Tomota, M. Strum, J.W. Morris Jr., Metall. Trans. A 17 (1986) 537.
[16] T. Sawaguchi, P. Sahu, T. Kikuchi, K. Ogawa, S. Kajiwara, A. Kushibe, M. Higashino, T. Ogawa, Scripta Mater. 54 (2006) 1885.
[17] T. Sawaguchi, L.G. Bujoreanu, T. Kikuchi, K. Ogawa, F. Yin, ISIJ Int. 48 (1) (2008) 99.
[18] S. Mahajan, C.S. Pande, M.A. Iman, B.B. Rath, Acta Mater. 45 (1997) 2633.
[19] M. Koyama, M. Murakami, K. Ogawa, T. Kikuchi, T. Sawaguchi, Mater. Trans. 49 (2008), doi:10.2320/matertrans.MRA2007321.
[20] Z. Xie, Y. Liu, J. Van Humbeeck, Acta Mater. 46 (1998) 1989.
[21] Y. Liu, Z. Xie, J. Van Humbeeck, L. Delaey, Acta Mater. 46 (1998) 4325.